Protein Science (1999), *8*:1484–1491. Cambridge University Press. Printed in the USA.

Conformational properties of native sperm whale apomyoglobin in solution

JULIETTE T.J. LECOMTE, STEVEN F. SUKITS, SHIBANI BHATTACHARYA, AND CHRISTOPHER J. FALZONE

Department of Chemistry and the Center for Biomolecular Structure and Function, The Pennsylvania State University, University Park, Pennsylvania 16802

(RECEIVED September 15, 1998; ACCEPTED March 4, 1999)

Abstract

Apomyoglobin from sperm whale is often used for studies of ligand binding, protein folding, and protein stability. In an effort to describe its conformational properties in solution, homonuclear and heteronuclear (^{13}C and ^{15}N) NMR methods were applied to the protein in its native state. Assignments were confirmed for nuclear Overhauser effects (NOEs) involving side chain and backbone protons in the folded regions of the structure. These NOEs were used to derive distance restraints. The shifts induced by the hydrophobic dye 8-anilino-1-naphthalenesulfonic acid (ANS) were inspected in the regions remote from its binding site and served as an indicator of conformational flexibility. $^{3}J_{\alpha\text{H-NH}}$ values were obtained to assess dihedral angle averaging and to provide additional restraints. A family of structures was calculated with X-PLOR and an ab initio simulated annealing protocol using holomyoglobin as a template. Where the structure appeared well defined by chemical shift, line width, ANS perturbation, and density of NOEs, the low resolution model of apomyoglobin provides a valid approximation for the structure. The new model offers an improved representation of the folded regions of the protein, which encompass the A, B, E, helices as well as parts of the G and H helices. Regions that are less well defined at this stage of calculations include the CD corner and the end of the H-helix. The EF-F-FG segment remains uncharacterized.

Keywords: ANS; apomyoglobin; myoglobin; NMR; partially folded protein

Hemoproteins of the *b* type constitute a group of proteins including, among others, cytochrome b_{562}, cytochrome b_5, and myoglobin. These three proteins each contain a single iron-porphyrin IX prosthetic group and behave as typical globular species, with a stable, well-defined structure capable of cooperative thermal unfolding (Pfeil & Bendzko, 1980; Privalov et al., 1986; Robinson et al., 1998). In their apoprotein form, they display lower thermodynamic stability than in their holoprotein form (Griko et al., 1988; Pfeil, 1993; Robinson et al., 1998) and an open, partially folded heme-binding site (Feng et al., 1994; Eliezer & Wright, 1996; Falzone et al., 1996; Lecomte et al., 1996). Myoglobin (Mb) from sperm whale (*Physeter catodon*) is the most studied of the three proteins. It contains, embedded within its 153 residues, a *b* heme group whose function is to bind oxygen for storage in red muscles. Sperm whale Mb folds into eight helices labeled A through H (Fig. 1A). The heme iron is coordinated to the protein matrix through the "proximal" histidine, located in the F helix. In vitro heme binding to the Mb apoprotein occurs in a rapid bimolecular association reaction ($k_{on} \approx 10^8\ M^{-1}\ s^{-1}$) independent of the apoprotein primary structure (Hargrove et al., 1996a). Heme loss is slow, depends on primary structure, and controls heme affinity. Sperm whale Mb loses heme with a rate constant of $10^{-6}\ s^{-1}$, yielding a dissociation constant on the order of 10^{-14} (Hargrove et al., 1996b).

The holoprotein reconstitution reaction proceeds via a unique mechanism. A few seconds after heme addition, a nearly 1:1 mixture of two holoprotein forms is observed. These kinetically trapped isomers differ by a 180° rotation of the porphyrin plane relative to the protein (Fig. 1A,B; La Mar et al., 1978, 1983). Subsequent heme rotation, apparently intramolecular, eventually produces the thermodynamic proportions of the two forms (≈9:1 in the sperm whale protein; La Mar et al., 1984). The features enabling the apoprotein to select for only two heme orientations prior to proximal histidine ligation have not been described.

Reprint requests to: Juliette T.J. Lecomte, Chemistry Department, The Pennsylvania State University, 152 Davey Laboratory, University Park, Pennsylvania 16802; e-mail: jtl1@psu.edu.

Abbreviations: ANS, 8-anilino-1-naphthalenesulfonic acid; apoMb, apomyoglobin; CD, circular dichroism; DSS, sodium 2,2-dimethyl-2-silapentane-5-sulfonate; HMQC, heteronuclear multiple quantum coherence; HSQC, heteronuclear single quantum coherence; Mb, myoglobin; MbCO, carbonmonoxymyoglobin; metaquoMb, metaquomyoglobin; NOE, nuclear Overhauser effect; NOESY, two-dimensional nuclear Overhauser spectroscopy; RMS, root-mean-square; RMSD, root-mean-square deviation; TOCSY, total correlation spectroscopy; TPPI, time proportional phase incrementation.

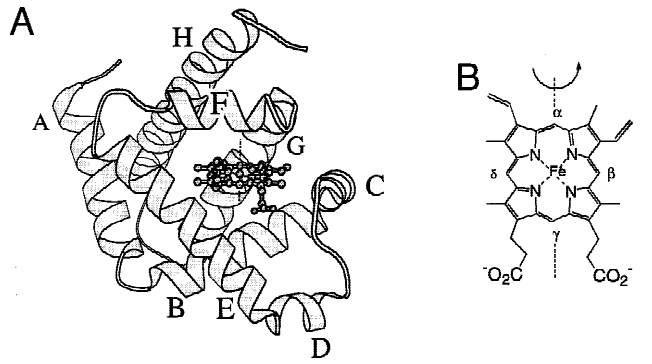

Fig. 1. A: Schematic representation of the three-dimensional structure of holomyoglobin, as determined by X-ray diffraction methods. The MOLSCRIPT drawing (Kraulis, 1991) is based on the coordinate file 4mbn.pdb (Takano, 1977a, 1984). The eight helices of Mb are labeled A through H. The heme binding site is formed by the F-helix (containing the coordinating or proximal histidine, His93 or F8) and the E-helix (containing the distal histidine, His64 or E7). **B:** The heme group is shown with sticks and balls; its propionate substituents point toward solvent, whereas the vinyl substituents point toward the inside of the protein. Approximately 10% of the myoglobin molecules have the heme rotated by 180° with respect to the axis that passes through the α and γ meso positions (La Mar et al., 1983).

Aside from issues of prosthetic group binding, there is interest in apoMb because it adopts distinct thermodynamic states under different pH, salt, and temperature conditions (Griko & Privalov, 1994; Barrick & Baldwin, 1993). This has promoted it as a well-suited protein for original physico-chemical investigations of the determinants of protein folding and stability (Ballew et al., 1996a; Gilmanshin et al., 1997; Eliezer et al., 1998; Ha & Loh, 1998; Haliloglu & Bahar, 1998). However, the combination of low stability, structural disruption, and internal motions that defines partially folded proteins makes native apoMb a difficult subject for detailed structural studies, and it remains insufficiently characterized.

NMR experiments have provided a wealth of information. The secondary structure apparent in CD spectra (Breslow et al., 1965) has been detected through nuclear Overhauser effects (NOEs) typical of helices and turns (Lecomte et al., 1996). Protection factors for backbone amide hydrogens have indicated hydrogen bonding in several helices (Hughson et al., 1990). Analyses of the $^{13}C\alpha$ chemical shift index complement these studies (Eliezer et al., 1998). Tertiary structure, manifested in a change in heat capacity upon unfolding (Griko et al., 1988), has been identified through NOEs among buried residues (Cocco & Lecomte, 1990; Lecomte et al., 1996) and through the ionization constants of histidines (Cocco et al., 1992).

A distinctive property of native apoMb is the juxtaposition of folded parts and regions less conformationally restrained. The latter include the proximal side of the heme-binding site, where the polypeptide chain is endowed with motions on a time scale preventing NMR detection (Eliezer & Wright, 1996; Lecomte et al., 1996). Proteolysis experiments reveal enhanced susceptibility in the F-helix (Fontana et al., 1997) and in the CD corner and C-terminal end of the H-helix (Zhong et al., 1995). Toward the C-terminus of the protein, the ^{1}H NMR lines are broad and indicative of helix fraying. The folded secondary elements include at least portions of the A, B, C, D, E, G, and H helices. The ABGH interface (Fig. 1A) constitutes a stable nucleus, most of which is formed early in the refolding of the apoprotein (Jennings & Wright, 1993).

In previous ^{1}H NMR work, a low resolution model of the ABGH interface was generated using NOEs in a simulated annealing procedure of structure determination (Lecomte et al., 1996). NMR models are comprised of structures compatible with the restraints used to produce them. When these early apoMb structures were superimposed locally over the segments defining the D and E helices, it became apparent that the model also reflected some of the helical propensity in these elements and that the structured nucleus is larger than the ABGH core. However, the disposition of the D and E helices relative to the rest of the protein—the tertiary structure—was unclear. Thus, the original model was of low resolution and restricted to a smaller part of the molecule than actually folded.

The information available from solution state NMR techniques applied to partially folded and unfolded proteins is derived from chemical shift comparisons, inter-residue distances viewed by NOEs or paramagnetic relaxation, and backbone dynamics (Shortle, 1996; Dyson & Wright, 1998). Extending these results to complete structure calculations involves incorporating the stochastic nature of the conformational ensembles into the modeling of macroscopic observables. The problem is simplified for partly folded systems where the propensity for native contacts is large and the segmental motions characteristic of random coils are restricted to short independent segments of the polypeptide chain (Feng et al., 1994; Falzone et al., 1996; Riek et al., 1997). In those cases, a useful representation of the folded core of the protein can be obtained.

The heme binding site of Mb has affinity for the hydrophobic dye 8-anilino-1-naphthalenesulfonic acid (ANS) (Stryer, 1965). It is shown that the ANS complex helps to determine which portions of apoMb are amenable to standard structural calculations. The ANS data, combined with heteronuclear NMR data collected on uniformly ^{13}C,^{15}N- and ^{15}N-labeled apoMb, allowed for an evaluation of the conformational properties of apoMb in solution and a continuation of the tertiary structure determination.

Results

Homonuclear data have been collected on sperm whale apoMb in its native state (Lecomte et al., 1996, and references therein). The quality of the two-dimensional proton spectra is such that relatively few NOE cross peaks can be unambiguously assigned. As a result, only a limited set of restraints was used in previous modeling efforts (Lecomte et al., 1996). In this work, three-dimensional NMR data sets were acquired on ^{15}N- and ^{13}C,^{15}N-labeled apomyoglobin to ascertain the origin of prominent cross peaks in the NOESY spectra. As observed by others (Eliezer & Wright, 1996), the relaxation properties of the ^{13}C nuclei in apoMb are unfavorable, so that the improvement due to the double labeling is limited. Thus, although the ^{13}C,^{15}N data were helpful in the assignment step, only the ^{15}N data (^{1}H-^{15}N NOESY-HSQC) were used to derive structural restraints. Not all cross peaks could be identified and other methods were considered to complement the NOE data.

Proton chemical shifts can be used as a comparative indicator of structure. Figure 2 shows sequential plots of chemical shift differences between apoMb and the random coil (Fig. 2A), and between apoMb and the carbonmonoxy complex of reduced Mb (MbCO, Fig. 2B). The MbCO chemical shifts (Kao & Lecomte, 1993; Osapay et al., 1994; Thèriault et al., 1994) were corrected for the heme ring current contribution as described elsewhere (Kao & Lecomte, 1993). On average, the apoprotein shifts correlate better with the holoprotein shifts than with the random shifts. There are

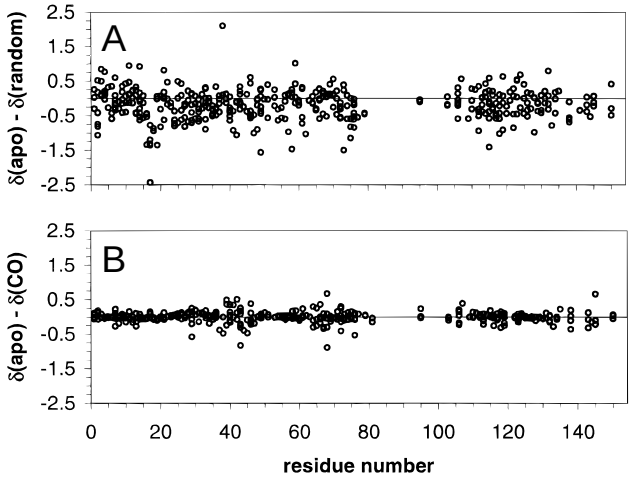

Fig. 2. Comparison of the ^{1}H chemical shift (ppm) of assigned resonances in apoMb and (**A**) random coil (Bundi & Wüthrich, 1979), δ(apo) − δ(random) and (**B**) MbCO, δ(apo) − δ(CO), after correction for the ring current induced by the heme group. Values for the nonrecombinant protein are used for Val1 and Leu2.

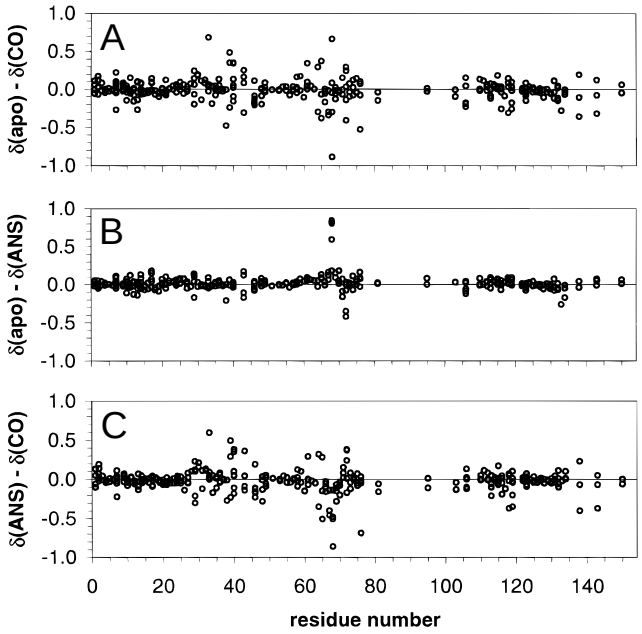

Fig. 3. Comparison of the ^{1}H chemical shift (ppm) of assigned resonances in three forms of Mb: MbCO, apoMb, and apoMb complexed with ANS. **A:** A subset of the data points shown in Figure 2B, δ(apo) − δ(CO). Only those resonances identified in the three forms of the protein are included. **B:** δ(apo) − δ(ANS). **C:** δ(ANS) − δ(CO). The shifts induced by ANS are felt throughout the chain. **C** compared to **A** suggests that the deviation from the holoprotein shifts is lower in the presence of the bound ANS.

a number of outliers in the holoprotein plot (Fig. 2B). Where the calculated heme ring current shift is high, the discrepancy between corrected CO shifts and apoMb shifts could be due to either a structural perturbation or an incorrect estimate of the ring current shift. The latter is particularly likely if the ring current shift is larger than an empirical 1 ppm cut off. Most outliers fall in this category.

Overall, Figure 2 reflects the strong tendency of the apoprotein to adopt the holoprotein conformation. However, this alone is insufficient to assess the structure and its flexibility. To investigate the conformational properties of the apoprotein, the chemical shift perturbations induced by ANS were inspected. ANS binds weakly to the heme site (Stryer, 1965) and is in dipolar contact with E helix residues His64, Thr67, Val68, and Ala71 (Cocco & Lecomte, 1994; this work). A similar set of interactions is observed in horse apoMb (His64, Val67, Val68, and Ala71). The ANS complex yields better resolved spectra than the free apoprotein, likely because of a redistribution of conformer populations into a smaller number of states.

ANS, like the heme group, causes two types of shift perturbations: direct, for the residues in contact and those within ring current range, and indirect, through conformational rearrangement. Figure 3 summarizes the effect of ANS on apoMb. Panel A contains the chemical shift difference δ(apoMb) − δ(MbCO) for reference. The same set of resonances is used in Figure 3B to show δ(apoMb) − δ(apoMb ANS). In Figure 3B, most chemical shift differences are small and suggest that the sharpening of the lines is not accompanied by a major structural change. A comparison of δ(apoMb ANS) − δ(MbCO) (Fig. 3C) with δ(apoMb) − δ(MbCO) (Fig. 3A) displays a slight decrease in scatter where the direct influence of ANS is expected to be negligible. This is apparent from residue 10 to 30 (standard deviation of the shift differences changing from 8.3×10^{-2} in 3A to 7.3×10^{-2} in Fig. 3C) and from residue 122 to 130 (standard deviation of the shift differences changing from 4.4×10^{-2} in 3A to 3.1×10^{-2} in Fig. 3C). Figure 3C thus hints at local refolding into a holo-like conformation. Because ANS binding produces an apo state resembling the free apo state structurally, but improved spectrally, the ANS complex was used to resolve cross peak ambiguities.

The line width, effect of ANS, and hydrogen exchange data can be explained with an ensemble of interconverting apoMb conformations, and caution that a structural determination should make allowance for enhanced fluctuations about an average. To probe this further, *J*-modulated HSQC data were collected to obtain $^3J_{\alpha\text{H-NH}}$ values (Neri et al., 1990). For α secondary structure, $^3J_{\alpha\text{H-NH}}$ is generally below 5 Hz, whereas for an extended conformation, the value is larger than 8 Hz. Values comprised between 6 and 8 Hz suggest possible conformational averaging.

In the *J*-modulated experiments, an 8-Hz coupling implies that the NH cross peak will change sign near a modulation time of 60 ms, and sooner if $^3J_{\alpha\text{H-NH}}$ is larger (see Equation 1 in Materials and methods). In apoMb, only a few NH cross peaks show a sign reversal indicative of $^3J_{\alpha\text{H-NH}} > 8$ Hz. This is consistent with a protein expected to contain rare φ,ψ pairs in the β region of the Ramachandran plot. Small coupling constants are difficult to determine by this method because of relaxation during the modulation delay. $^3J_{\alpha\text{H-NH}}$ values were obtained within an acceptable precision (better than 1 Hz) from 32 NH cross peaks, giving φ angles as indicated in Figure 4. The majority of remaining $^3J_{\alpha\text{H-NH}}$ values have a larger uncertainty, but are nevertheless below 6 Hz.

The ensemble of experimental data suggests that regions of apoMb are sufficiently restricted conformationally to justify the continuation of model building. Structural calculations were therefore pursued with an ab initio simulated annealing protocol (Nilges et al., 1991). A total of 680 NOE restraints were applied, which were unaffected by the addition of ANS. The restraints are concentrated in the regions 1 to 76 and 104 to 136 of apoMb, as shown

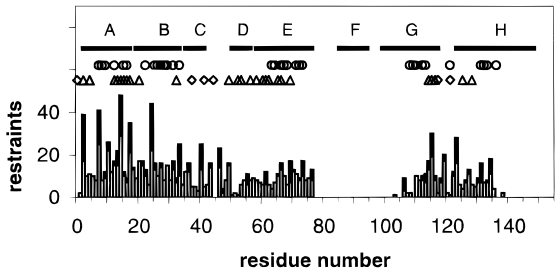

Fig. 4. Restraints used in the structural calculations: The open bars represent the number of short- and medium-range NOE distances ($|i - j| \leq 4$); closed bars represent the number of long-range NOE distances ($|i - j| > 4$); (○), NH participating in H-bond with the backbone CO at $i - 4$; (◇) backbone dihedral angle $\varphi = -130°$; (△) $\varphi = -50°$. Solid horizontal bars delineate the helices in the holoprotein.

in Figure 4. The initial model positions several backbone CO and NH moieties within H-bonding range. The H-bonds inferred from the structures involve the NHs with protection factors higher than 1,000. A limited set of H-bond restraints was applied in a subsequent round of calculations. Only amides giving rise to signals detectable in a NOESY spectrum collected on freshly dissolved protein in ^2H_2O were used at this stage. The structures so obtained do not account well for the known pattern of backbone hydrogen exchange protection. For example, a section of the E helix, known to undergo slow exchange (Hughson et al., 1990), has NHs that are accessible to solvent in many structures. The H-bonds for the slowly exchanging amides were added in these regions in a final round of calculations. This procedure, which biases the structure toward that of the holoprotein, is consistent with all the experimental data and introduces no violation.

The simulated annealing (SA) protocol yielded 80 structures out of 100 belonging to a continuum of X-PLOR energies as defined by Nilges and coworkers (Abseher et al., 1998). Figure 5A contains 20 Cα traces chosen across this ensemble of 80 structures to offer a representation of the sampled conformational space. Only the regions folded by the NMR data are included in Figure 5A. The SA model can be evaluated with the RMSDs of the Cα positions. In Figure 6A, these deviations are shown for three separate superimpositions on the average of three stretches of the protein: Cα for residues 2 to 36, 59 to 76, and 104 to 136. The low values reflect the formation of elements of secondary structure. If the fit is carried out for the same regions simultaneously over their average, the RMSDs increase moderately and become more scattered (Fig. 6B, dashed lines). The small increase supports that the local elements and their relative disposition are now contained in the data. The RMSDs can also be calculated with respect to the holoprotein Cα coordinates (Fig. 6B, solid lines). At this low resolution, the differences are comparable to the differences within the family of structures and may not be significant.

Discussion

The NMR parameters with and without ANS indicate that the N state of sperm whale apoMb consists of related conformations exchanging on an intermediate to fast chemical shift time scale.

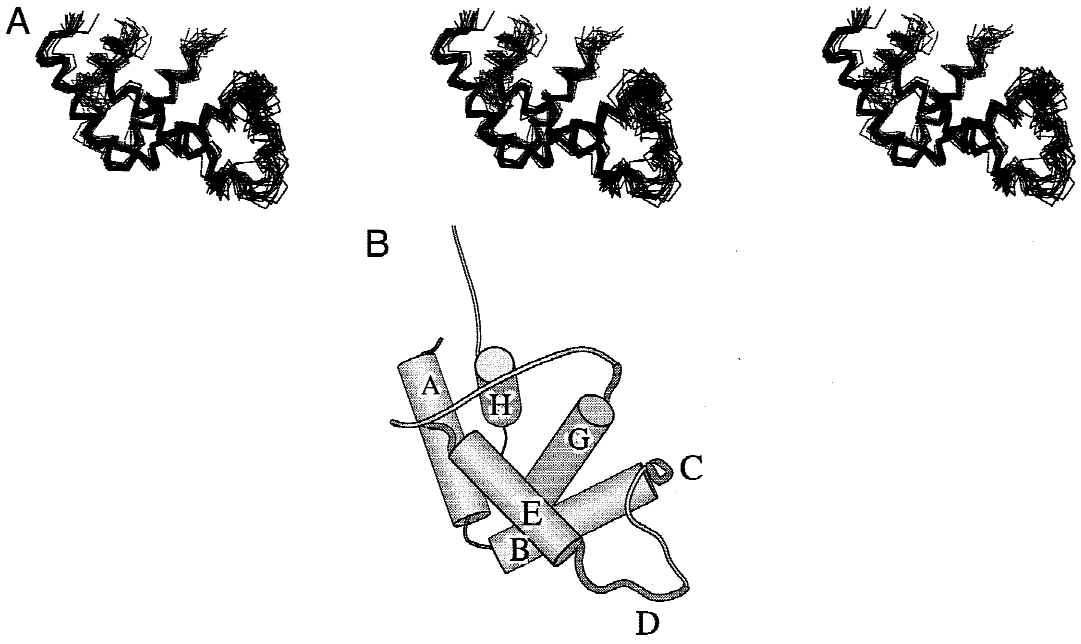

Fig. 5. A: Backbone model of apoMb derived from NMR simulated annealing structural calculations. Twenty Cα traces are superimposed in a stereo triptych. The structures were chosen to sample the continuum of X-PLOR energies (see text). Alignment was carried out on the average Cα coordinates simultaneously in the regions 2 to 35, 59 to 76, and 104 to 136. Only the segments of polypeptide 1 to 76 and 104 to 136 are shown. The orientation is similar to that of Figure 1, with the E-helix in front. The G–H face is behind and represented in dashed lines. **B:** Cartoon representation of apoMb, generated from the average apoMb structure. Helical regions are represented as cylinders. Helical turns that are sampled in fewer than half the structures are marked in gray coil. This summary diagram does not take into account the uneven degree of determination and conformational sampling throughout the structure.

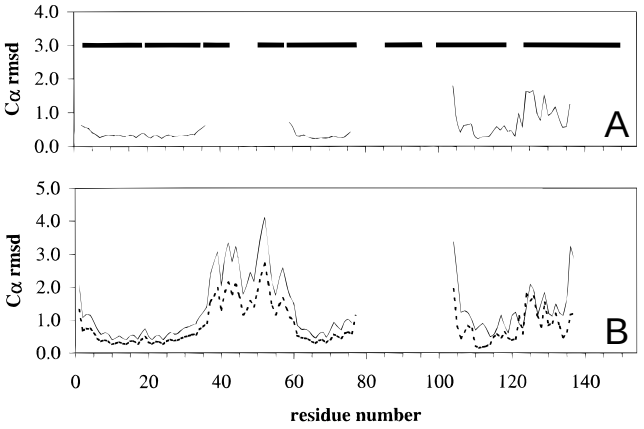

Fig. 6. RMSDs for Cα coordinates in the structure of apoMb. **A:** A set of 80 X-PLOR structures in the continuum of energy were superimposed individually on the average of three different segments: 2–35, 59–76, and 104–136. Solid bars denote the helices in the holoprotein. **B:** Deviations calculated when the superimposition is performed on the average structure obtained for the same three segments at the same time (dashed lines) and when the superposition is carried out over the holoprotein structure (solid lines). The chemical shifts suggest that the Cα RMSD shown in **B** for the C–CD–D region is in part artifactual.

This implies a potentially broad range of rates and raises the possibility that the relationship between NOE cross peak intensity and internuclear distance is not uniform throughout the structure (Neuhaus & Williamson, 1989). Where the inter-residue NOE density is low, and large amplitude fluctuations are suspected, the structure derived from the NOEs is likely not to be accurate. Where the NOE density is high and the intensities and widths are comparable to those in the holoprotein, a calculation can provide an acceptable approximation of the gross structure.

As expected, because of the nature of the apoMb native state and the small number of restraints, several conformations are acceptable (Fig. 5A). Lack of data remains a limitation particularly in the flexible regions, which are incompletely described. To summarize the features of the apoMb model in comparison to Mb, a cartoon was prepared with the *average* Cα coordinates of the structures (Fig. 5B). The cylinders represent elements of secondary structure that are formed in all individual structures. The EF-F-FG loop and the end of the H helix are averaged to featureless stretches and are shown in thin lines. Figure 5B is to be viewed with the family of structures shown in Figure 5A as a reminder that high resolution information cannot be derived uniformly from the model. For example, the cartoon suggests a reorientation of the H-helix; this could be the result of the current restraint distribution, which does not confine the end of the helix and exaggerates small angular error in the ABGH interface. In addition, chemical shifts, NOEs, and dihedral angles provide no information on the correlation of the various motions. The local folding–unfolding processes occurring in adjacent segments of the protein could be independent even though the global unfolding of apoMb is cooperative. Such subdomain behavior has been observed in apocytochrome b_{562} where detailed hydrogen exchange studies have revealed three regions of subglobal cooperativity (Fuentes & Wand, 1998).

Figure 5 captures several coarse features of apoMb and extends the knowledge of the structure. An earlier study, using ^{1}H-NOE methods, characterized the ABGH interface (Lecomte et al., 1996). The A-helix, AB-turn, and B-helix, regions minimally affected by ANS binding, are now well defined. The C-helix appears blurrier than the A- and B-helices because of a low restraint count due in part to resonance overlap. However, some degree of fluctuation is supported by weak NOEs and the chemical shift data of Wright and coworkers, which suggest 75% helicity in this region (Eliezer et al., 1998). The CD-turn displays high B-factors in the holoprotein (Cheng & Schoenborn, 1991; Yang & Phillips, 1996) and is underdetermined in the apoprotein. Heteronuclear ^{1}H-^{15}N NOE data were collected to assess the mobility of the backbone. The results are essentially as reported by others (Eliezer et al., 1998), showing a depression of the effect in the CD region and indicating internal motions on the subnanosecond time scale. The chemical shift scatter in Figure 3 also supports a greater conformational variability in this region. Short-range side-chain interactions, as well as the pK_a of His36 and His48 (8 and 5, respectively, in both apoMb and holoMb; Cocco et al., 1992), indicate that the local structure is at least partially in place in this region. Chemical shift degeneracy in the D-helix and beginning of the E-helix prevents the detection of some of the backbone NOEs necessary to refine the structure. For the rest of the E-helix, the chemical shift argument (Fig. 2B) indicates limited structural rearrangement. On average, the E-helix appears positioned with respect to the ABGH interface as in the holoprotein.

The F-helix residues belong to a region devoid of long-range restraints, extending from residues 77 to 104 and encompassing the EF-turn, the F-helix, the FG-turn, and the beginning of the G-helix. Beyond the first turn of the G-helix, structural evidence is recovered as the helix docks against the AB region. The GH turn is maintained as well as most of the H-helix. The data at the end of the H-helix point to structural alterations (see below). It is noteworthy that many globin sequences end at H20 (Ala143 in sperm whale Mb; Bashford et al., 1987) and only H15 and H19 are buried at a helical interface.

Within the limitations of the model, there is confirmation for altered packing in two regions of the protein. In the C-helix, the chemical shift scatter with respect to the holoprotein is larger than in the A-B helices. This can be due to the alteration of the helix itself or the nearby regions. For example, after correction for heme ring current shift and under an isostructural assumption for holo and apoMb, the methyl group of Thr39 (C4) would resonate approximately at 0.9 ppm. This upfield-shifted value compared to the random value of 1.2 ppm is caused by Tyr103 (G3). The observed 1.35 ppm shift in the apoprotein can be explained in terms of a change in the relative orientation of the G3 and C3 side chains in the apoprotein.

In the F-helix, the methyl group of Thr95 is tentatively assigned at 1.1 ppm, but the heme ring current shift correction calculated on the basis of a constant structure fails to reproduce the experimental shift. The same holds for Ala94, whose chemical shift in the holoprotein is strongly influenced by Tyr146 and Tyr151. No alanine resonance is found at the predicted chemical shift of 0.6 ppm. Given that all 17 alanines can be detected, this provides additional evidence for the disruption of contacts between the F-helix and the end of the H-helix. ^{13}Cα chemical shift indices (Eliezer et al., 1998) are consistent with this conclusion.

Global properties of the molecule emerge from the model. Mb, a disk of dimensions ~48 Å × 40 Å × 22 Å, expands to a less ordered state upon heme removal. Solution X-ray scattering data collected on horse apomyoglobin indicate an increase in the largest dimension of the protein to 63 Å (Kataoka et al., 1995). The

structures derived for sperm whale apoMb allow for an increase in anisotropy through the regions not included in Figure 5A; the main change in dimension would take place along the axis of the H-helix. The NMR model also imposes restrictions on the average size of the molecule. The radius of gyration of the 20 structures was evaluated with the program HYDRO (Venable & Pastor, 1988), by representing each residue by a bead (radius 3.4 Å) centered at the Cα coordinates. The nonhydrated radius has an average value of 18.5 Å. This is in comparison to 15.4 Å for the holoprotein. The experimental values obtained by X-ray scattering on horse myoglobin are comparable: 19.7 Å (apoprotein) and 17.5 Å (holoprotein) (Kataoka et al., 1995).

The apoprotein model is relevant to the mechanism of in vitro heme binding (Kawamura-Konishi et al., 1988). At this stage, it is possible to speculate on the earliest phase of recognition. Initial positioning of the heme in its high affinity site necessitates the hydrophobic surface on the distal side (E-helix). All heme orientations but two are then rapidly eliminated to balance electrostatic and steric interactions between the heme group and the protein matrix. Preorganized or readily recruited residues in contact with the propionate and the vinyl side chains, among which the model suggests Thr39 (C4), Phe43 (CD1), Arg45 (CD3), Val68 (E11), Leu72 (E15), and Ile107 (G8), could guide this rapid selection. Further protein folding and proximal histidine coordination then occur, retarding the heme rearrangement into the major isomer.

ApoMb and apocytochrome b_5 (Falzone et al., 1996) show that a heme pocket can be constructed with two dynamically different faces. In apoMb, the distal side is folded and the proximal side is fluctuating. Amino acid sequence analyses and structural comparisons relate the distal face of apoMb to the unfolded face of apocytochrome b_5 (Runnegar, 1984). If this relationship is valid, which of the face is folded is not essential. Perhaps more important in these cases is that the heme binding sites are made of helices. Helices satisfy shape complementarity requirements but they also are local elements of secondary structure whose unfolding may be rapid (Ballew et al., 1996b; Gilmanshin et al., 1997). Helix unwinding provides a mechanism for loosening the heme pocket without severe tertiary structure consequences. This could endow the protein with advantageous thermodynamic and dynamic properties.

ApoMb has so far eluded high resolution characterization. Spectral indicators were used here to examine the validity of applying standard structural methods to it. Although the location of secondary structure has been reasonably well established, the tertiary structure is still not entirely contained in the current representation. A more complete description will be likely to require the interpretation of backbone and side-chain dynamics in an exchanging system. Nevertheless, the new model does begin to reveal where tertiary contacts are maintained or can be adopted by apoMb. As such, it is a useful structural view of a much studied system.

Materials and methods

Protein samples

Sperm whale (*Physeter catodon*) myoglobin was either purchased from Sigma (St. Louis, Missouri) and used without further purification, or produced in *Escherichia coli* cell strain BL21 (DE3) using a pET13d plasmid containing the myoglobin gene (a gift from Dr. Fang Shu). The ^{15}N- and ^{13}C,^{15}N-labeled proteins were prepared as reported previously (Bhattacharya et al., 1997). All apoMb samples were obtained by the cold butanone method (Teale, 1959).

NMR samples

The solutions were approximately 1 mM in protein and 10 mM in acetate buffer, pH 5.7, with added ^2H_2O to yield a 90% H_2O/10% ^2H_2O solution. The pH was adjusted using 0.1 M NaOH and 0.1 M HCl. The apoMb ANS complex and MbCO complex were prepared as previously described (Cocco & Lecomte, 1994).

NMR experiments

Data were recorded on a Bruker AMX2-500 spectrometer operating in the quadrature mode at a ^{1}H frequency of 500.13 MHz. The probe temperature was 304 K. Proton data (^{1}H-^{1}H NOESY and ^{1}H-^{1}H TOCSY) were acquired as described elsewhere (Lecomte et al., 1996).

Heteronuclear spectra were collected using triple-resonance (^{1}H/^{15}N/^{13}C) z-gradient shielded probe. Solvent suppression was achieved through the WATERGATE scheme (Sklenár et al., 1993). The following three-dimensional experiments were run with their indicated spectral widths and complex data points (*) acquired for dimensions t1, t2, and t3, respectively: ^{1}H-^{15}N TOCSY-HSQC (^{1}H: 6,024 Hz, 64*; ^{15}N: 1,500 Hz, 32*; ^{1}H: 7,042 Hz, 2,048*; mixing time 44 ms) and ^{1}H-^{15}N NOESY- HSQC (^{1}H: 6,024 Hz, 64*; ^{15}N: 1,500 Hz, 32*; ^{1}H: 7,042 Hz, 2,048*; mixing time 80 ms) (modified from Cavanagh et al., 1996); ^{1}H-^{13}C HCCH-TOCSY (Kay et al., 1993) and COSY (Ikura et al., 1991) (^{1}H: 4,000 Hz, 64*; ^{13}C: 8,000 Hz, 32*; ^{1}H: 4,000 Hz, 512*); ^{1}H-^{13}C NOESY-HSQC (^{1}H: 6,024 Hz, 64*; ^{13}C: 7,575 Hz, 32*; ^{1}H: 6,024 Hz, 512*) (Muhandiram et al., 1993); HNCA (^{15}N: 1,700 Hz, 36*; ^{13}C: 2,500 Hz, 48*; ^{1}H: 6,024 Hz, 512*) (modified from Grzesiek & Bax, 1992c), CBCANH (^{13}C: 7,142 Hz, 50*, ^{15}N: 1,700 Hz, 24*, ^{1}H: 7,042 Hz, 512*) (Grzesiek & Bax, 1992b) and CBCA(CO)NH (^{13}C: 7,142 Hz, 50*, ^{15}N: 1,700 Hz, 25*, ^{1}H: 7,042 Hz, 512*) (modified from Grzesiek & Bax, 1992a). Quadrature detection in the indirect dimensions was achieved using TPPI-States for all of these experiments (Marion et al., 1989).

A set of eight *J*-modulated ^{1}H-^{15}N HSQC experiments were performed with mixing times ranging from 52 to 116 ms for measuring $^3J_{\alpha\text{H-NH}}$ coupling constants (Neri et al., 1990). Parameters were ^{1}H: 7,042 Hz, 2,048* and ^{15}N: 1,500 Hz, 200*. The ^{1}H carrier was placed on the water resonance and the ^{15}N carrier was placed at 118 ppm. ^{1}H-^{15}N heteronuclear NOE were collected at pH 6.2, 304 K with WATERGATE suppression of the water signal. Parameters were ^{1}H: 7,042 Hz, 2,048* and ^{15}N: 1,500 Hz, 128*. Spectral width and digital resolution were as for the *J* experiment. The total recycle time was 4 s; irradiation was applied to the center of the amide region for 3 s with a WALTZ-16 scheme. Quadrature was achieved with TPPI.

Data were processed with FELIX (Molecular Simulations Inc., San Diego, California). Data collected in 90% H_2O/10% ^2H_2O were subjected to a 20 Hz sinebell-based convolution function to suppress the solvent. Shifted squared sinebell (45 to 60°) were applied in both dimensions. Data were zero filled once in the indirect dimensions. Linear prediction was used in the three-dimensional ^{1}H-^{15}N NOESY-HSQC experiment in the ^{15}N dimension (24 points). The proton chemical shifts were indirectly referenced to DSS through the water signal with temperature correction (Wishart et al., 1995). Nitrogen shifts were referenced

indirectly to ammonium chloride (Live et al., 1984) and carbon to DSS. Chemical shifts were essentially as reported previously by us and Wright and coworkers (Eliezer & Wright, 1996; Eliezer et al., 1998), save for minor variations due to sample conditions. Assignments in the ANS complex were obtained by homonuclear methods.

In the *J*-modulated experiment, the intensity of the cross peaks was measured and plotted as a function of the mixing time, τ. Nonlinear least-squares fitting was performed to Equation 1

$$I(\tau) = I_0 \times \cos(\pi^3 J_{\alpha\text{H-NH}}\tau) \times \exp(-\tau/T), \quad (1)$$

where $I(\tau)$ is the intensity of the cross peak of interest at time τ; I_0 is the amplitude at $\tau = 0$ and T a relaxation parameter. A Karplus equation translated these measurements into estimates of the backbone dihedral angle φ. $^3J_{\alpha\text{H-NH}}$ restraints were considered only for those residues with a small error ($<\pm 1$ Hz) even if the upper bound of the value was below 6 Hz. This yielded 32 restraints.

Ring current shift calculations

The ring current shift exerted by aromatic side chains and heme group was calculated with the program previously used (Kao & Lecomte, 1993). Holoprotein coordinates were those of sperm whale MbCO (Protein Data Bank (PDB) file 2mb5; Cheng & Schoenborn, 1991) and metaquoMb (PDB file 4mbn; Takano, 1977a, 1984) to account for variations in the solid state coordinates.

Structural calculations

The structures were calculated with X-PLOR 3.84 (Brünger, 1992) with a protocol similar to that described previously (Lecomte et al., 1996). The proton NOESY data in ^2H_2O and H_2O, the ^{1}H-^{15}N NOESY-HSQC data, and the ^{1}H-^{13}C NOESY-HSQC data were analyzed to yield interproton restraints, applying to residues 1 to 76 and 104 to 136. The distance restraints were classified into weak, medium, and strong categories after calibration with Trp Cζ2H-CηH and Tyr CδH-CϵH cross peak volumes. The cross peaks were compared to the corresponding cross peaks in the ANS complex to ascertain that the distance was not affected by the binding. A change in distance would denote a flexible part of the structure and an unreliable constraint. The respective distance ranges for these three categories were 1.8 to 2.7 Å, 1.8 to 3.3 Å, and 1.8 to 5.0 Å. Methyl groups and ortho and meta protons of Phe and Tyr were treated as X-PLOR pseudoatoms with $\langle r^{-6}\rangle$ averaging; 0.5 Å was added to the upper bound and the allowable lower limit was unchanged. Stereospecific assignments were made arbitrarily on the basis of chemical shift then adjusted on the basis of resulting violations. H-bond restraints were included as described in the text. In addition, the hydrogen bonds presumed between the side chains of His24 and His119, as well as the side-chain to main-chain hydrogen bond between His24 and Asp20, were explicitly enforced. The NMR-silent H-bond between Glu38-NH and Glu38 carboxylate was not applied. The accepted restraints were: φ, 32; short-range distances (same residue), 247; medium-range distances ($1 < |i-j| \leq 4$), 292 and 64 from 32 H-bonds; long-range distances ($|i-j| > 4$): 141 and 2 from 1 long range H-bond. This is a total of 778 restraints, an increase of 70% compared to the previous calculations.

The calculations were performed with a restrained ab initio simulated annealing protocol (Nilges et al., 1991) starting from the X-ray coordinates of deoxyMb (5mbn.pdb; Takano, 1977b, 1984) with adjustment made for the tautomeric states of histidine residues (Bhattacharya et al., 1997). The resulting structures are independent of the myoglobin template coordinates. The initial SA temperature was 1,000 K. The duration of the high temperature stage was 120 ps and that of cooling stage was 60 ps, with time steps of 0.005 ps.

A total of 100 structures were sorted by X-PLOR energy; 80 of these defined an energy continuum and contained a low number of small violations (smaller than 0.2 Å), none systematic. The 20 structures represented in Figure 5A were selected from the energy sorted set of 80 (one every four) without consideration for the number of violations. The average violation for this random set is smaller than 0.1 Å. Four structures had a long-range violation between 0.2 and 0.5 Å. The equivalent resolution of the set, as evaluated by AQUA and PROCHECK-NMR (Laskowski et al., 1996), is 2.8 Å for the folded segments, corresponding to 71% of the φ,ψ pairs in the allowed regions of the Ramachandran plot, 25% in the additional allowed regions, and 3% in the generously allowed region. At this resolution, the differences between the apoprotein structure (where folded) and the holoprotein structure may not be significant. Time-averaged distance restraint calculations (Torda et al., 1990) were performed for residues 37 to 58 to obtain a view of the range of geometries allowed by the data (Nanzer et al., 1994). A 10 ps trajectory was generated from the lowest X-PLOR energy structure of the set over 10,000 frames. A total of 250 frames were extracted at regular interval for RMSD calculations. The values compare well with those obtained by including higher energy structures in the ensemble.

Acknowledgments

The National Institutes of Health supported this work with grant GM-54217. The authors wish to thank Drs. Melanie Cocco and Yung-Hsiang Kao for their initial participation in the project and the reviewers for useful comments.

References

Abseher R, Horstink L, Hilbers C, Nilges M. 1998. Essential spaces defined by NMR structure ensembles and molecular dynamics simulation show significant overlap. *Proteins Struct Funct Genet 31*:370–382.

Ballew RM, Sabelko J, Gruebele M. 1996a. Direct observation of fast protectin folding: The initial collapse of apoMb. *Proc Natl Acad Sci USA 93*:5759–5764.

Ballew RM, Sabelko J, Gruebele M. 1996b. Observation of distinct nanosecond and microsecond protein folding events. *Nat Struct Biol 3*:923–926.

Barrick D, Baldwin RL. 1993. Three-state analysis of sperm whale apomyoglobin folding. *Biochemistry 32*:3790–3796.

Bashford D, Chothia C, Lesk AM. 1987. Determinants of a protein fold. Unique features of the globin amino acid sequences. *J Mol Biol 196*:199–216.

Bhattacharya S, Sukits S, MacLaughlin KL, Lecomte JTJ. 1997. The tautomeric state of histidines in myoglobin. *Biophys J 73*:3230–3240.

Breslow E, Beychok S, Hardman KD, Gurd FRN. 1965. Relative conformations of sperm whale metmyoglobin and apomyoglobin in solution. *J Biol Chem 240*:304–309.

Brünger AT. 1992. *X-PLOR. Version 3.1. A system for X-ray crystallography and NMR*. New Haven, Connecticut: Yale University Press.

Bundi A, Wüthrich K. 1979. ^{1}H NMR parameters of the common amino acid residues measured in aqueous solutions of the linear tetrapeptides H-Gly-Gly-X-L-Ala-OH. *Biopolymers 18*:285–297.

Cavanagh J, Fairbrother WJ, Palmer AG, Skelton NJ. 1996. *Protein NMR spectroscopy. Principles and practice*. London: Academic Press.

Cheng X, Schoenborn BP. 1991. Neutron diffraction study of carbonmonoxymyoglobin. *J Mol Biol 220*:381–399.

Cocco MJ, Kao Y-H, Phillips AT, Lecomte JTJ. 1992. Structural comparison of apomyoglobin and metaquomyoglobin: pH titration of histidines by NMR spectroscopy. *Biochemistry 31*:6481–6491.

Cocco MJ, Lecomte JTJ. 1990. Characterization of hydrophobic cores in apomyoglobin: A proton NMR spectroscopy study. *Biochemistry 29*:11067–11072.

Cocco MJ, Lecomte JTJ. 1994. The native state of apomyoglobin described by proton NMR spectroscopy: Interaction with the radical HyTEMPO and the fluorescent dye ANS. *Protein Sci 3*:267–281.

Dyson HJ, Wright PE. 1998. Equilibrium NMR studies of unfolded and partially folded proteins. *Nat Struct Biol NMR Suppl 5*:499–503.

Eliezer D, Wright PE. 1996. Is apomyoglobin a molten globule? Structural characterization by NMR. *J Mol Biol 263*:531–538.

Eliezer D, Yao J, Dyson HJ, Wright PE. 1998. Structural and dynamic characterization of partially folded states of apomyoglobin and implications for protein folding. *Nature Struct Biol 5*:148–155.

Falzone CJ, Mayer MR, Whiteman EL, Moore CD, Lecomte JTJ. 1996. Design challenges for hemoproteins: The solution structure of apocytochrome b_5. *Biochemistry 35*:6519–6526.

Feng Y, Sligar SG, Wand AJ. 1994. Solution structure of apocytochrome b_{562}. *Nat Struct Biol 1*:30–35.

Fontana A, Zambonin M, Polverino de Laureto P, De Filippis V, Clementi A, Scaramella E. 1997. Probing the conformational state of apomyoglobin by limited proteolysis. *J Mol Biol 266*:223–230.

Fuentes EJ, Wand AJ. 1998. Local dynamics and stability of apocytochrome b_{562} examined by hydrogen exchange. *Biochemistry 37*:3687–3698.

Gilmanshin R, Williams S, Callender RH, Woodruff WH, Dyer RB. 1997. Fast events in protein folding: Relaxation dynamics of secondary and tertiary structure in native apomyoglobin. *Proc Natl Acad Sci USA 94*:3709–3713.

Griko YV, Privalov PL. 1994. Thermodynamic puzzle of apomyoglobin unfolding. *J Mol Biol 235*:1318–1325.

Griko YV, Privalov PL, Venyaminov SY, Kutyshenko VP. 1988. Thermodynamic study of the apomyoglobin structure. *J Mol Biol 202*:127–138.

Grzesiek S, Bax A. 1992a. Correlating backbone amide and side chain resonances in larger proteins by multiple relayed triple resonance NMR. *J Am Chem Soc 114*:6291–6293.

Grzesiek S, Bax A. 1992b. An efficient experiment for sequential backbone assignment of medium-sized isotopically enriched proteins. *J Magn Reson 99*:201–207.

Grzesiek S, Bax A. 1992c. Improved 3D triple-resonance NMR techniques applied to a 31 kDa protein. *J Magn Reson 96*:432–440.

Ha J-H, Loh SN. 1998. Changes in side chain packing during apomyoglobin folding characterized by pulsed thiol-disulfide exchange. *Nat Struct Biol 5*:730–737.

Haliloglu T, Bahar I. 1998. Coarse-grained simulations of conformational dynamics of proteins: Application to apomyoglobin. *Proteins 31*:271–281.

Hargrove MS, Barrick D, Olson JS. 1996a. The association rate constant for heme binding to globin is independent of protein structure. *Biochemistry 35*:11293–11299.

Hargrove MS, Wilkinson AJ, Olson JS. 1996b. Structural factors governing hemin dissociation from metmyoglobin. *Biochemistry 35*:11300–11309.

Hughson FM, Wright PE, Baldwin RL. 1990. Structural characterization of a partly folded apomyoglobin intermediate. *Science 249*:1544–1548.

Ikura M, Kay LE, Bax A. 1991. Improved three-dimensional ^{1}H-^{13}C-^{1}H correlation spectroscopy of a ^{13}C-labeled protein using constant-time evolution. *J Biomol NMR 1*:299–304.

Jennings PA, Wright PE. 1993. A molten globule intermediate formed early on the kinetic folding pathway of apomyoglobin. *Science 262*:892–896.

Kao Y-H, Lecomte JTJ. 1993. Determination of the zero-field splitting constant for proton NMR chemical shift analysis in metaquomyoglobin. The dipolar shift as a structural probe. *J Am Chem Soc 115*:9754–9762.

Kataoka M, Nishii I, Fujisawa T, Ueki T, Tokunaga F, Goto Y. 1995. Structural characterization of the molten globule and native states of apomyoglobin by solution X-ray scattering. *J Mol Biol 249*:215–228.

Kawamura-Konishi Y, Kihara H, Suzuki H. 1988. Reconstitution of myoglobin from apoprotein and heme, monitored by stopped-flow absorption, fluorescence and circular dichroism. *Eur J Biochem 170*:589–595.

Kay LE, Xu G-Y, Singer Au, Muhandiram DR, Forman-Kay JD. 1993. A gradient-enhanced HCCH-TOCSY experiment for recording side-chain ^{1}H and ^{13}C correlations in H_2O samples of proteins. *J Magn Reson B 101*:333–337.

Kraulis PJ. 1991. MOLSCRIPT: A program to produce both detailed and schematic plots of protein structures. *J Appl Crystallogr 24*:946–950.

La Mar GN, Budd DL, Viscio DB, Smith KM, Langry KC. 1978. Proton nuclear magnetic resonance characterization of heme disorder in hemoproteins. *Proc Natl Acad Sci USA 75*:5755–5759.

La Mar GN, Davis NL, Parish DW, Smith KM. 1983. Heme orientational disorder in reconstituted and native sperm whale myoglobin. Proton nuclear magnetic resonance characterizations by heme methyl deuterium labeling in the met-cyano protein. *J Mol Biol 168*:887–896.

La Mar GN, Toi H, Krishnamoorthi R. 1984. Proton NMR investigation of the rate and mechanism of heme rotation in sperm whale myoglobin: Evidence for intramolecular reorientation about a heme twofold axis. *J Am Chem Soc 106*:6395–6401.

Laskowski RA, Rullmannn JA, MacArthur MW, Kaptein R, Thornton JM. 1996. AQUA and PROCHECK-NMR: Programs for checking the quality of protein structures solved by NMR. *J Biomol NMR 8*:477–486.

Lecomte JTJ, Kao Y-H, Cocco MJ. 1996. The native state of apomyoglobin described by proton NMR spectroscopy: The A-B-G-H interface of wild-type sperm whale apomyoglobin. *Proteins Struct Funct Genet 25*:267–285.

Live DH, Davis DG, Agosta WC, Cowburn D. 1984. Long range hydrogen bond mediated effects in peptides: ^{15}N NMR study of gramicidin S in water and organic solvents. *J Am Chem Soc 106*:1939–1941.

Marion D, Ikura M, Tschudin R, Bax A. 1989. Rapid recording of 2D NMR spectra without phase cycling. Application to the study of hydrogen exchange in proteins. *J Magn Reson 85*:393–399.

Muhandiram DR, Farrow NA, Xu G-Y, Smallcombe SH, Kay LE. 1993. A gradient ^{13}C NOESY-HSQC experiment for recording NOESY spectra of ^{13}C-labeled proteins dissolved in H_2O. *J Magn Reson B 102*:317–321.

Nanzer AP, Poulsen FM, van Gunsteren WF, Torda AE. 1994. A reassessment of the structure of chymotrypsin inhibitor 2 (CI-2) using time-averaged NMR restraints. *Biochemistry 33*:14503–14511.

Neri D, Otting G, Wüthrich K. 1990. New nuclear magnetic resonance experiment for measurements of the vicinal coupling constants $^{3}J_{HNa}$ in proteins. *J Am Chem Soc 112*:3663–3665.

Neuhaus D, Williamson M. 1989. *The nuclear Overhauser effect in structural and conformational analysis*. New York: VCH.

Nilges M, Kuszewski J, Brünger AT. 1991. *Computational aspects of the study of biological macromolecules by NMR*. New York: Plenum Press.

Osapay K, Theriault Y, Wright PE, Case DA. 1994. Solution structure of carbonmonoxy myoglobin determined from nuclear magnetic resonance distance and chemical shift constraints. *J Mol Biol 244*:183–197.

Pfeil W. 1993. Thermodynamics of apocytochrome b_5 unfolding. *Protein Sci 2*:1497–1501.

Pfeil W, Bendzko P. 1980. Thermodynamic investigations of cytochrome b_5 unfolding. I. The tryptic fragment of cytochrome b_5. *Biochim Biophys Acta 626*:73–78.

Privalov PL, Griko YV, Venyaminov S, Kutyshenko VP. 1986. Cold denaturation of myoglobin. *J Mol Biol 190*:487–498.

Riek R, Hornemann S, Wider G, Glockshuber R, Wüthrich K. 1997. NMR characterization of the full-length recombinant murine prion protein, mPrP(23-231). *FEBS Lett 13*:282–288.

Robinson CR, Liu Y, O'Brien R, Sligar SG, Sturtevant JM. 1998. A differential scanning calorimetric study of the thermal unfolding of apo- and holocytochrome b_{562}. *Protein Sci 7*:961–965.

Runnegar B. 1984. Derivation of the globins from type *b* cytochromes. *J Mol Evol 21*:33–41.

Shortle DR. 1996. Structural analysis of non-native states of proteins by NMR. *Curr Opin Struct Biol 6*:24–30.

Sklenár V, Piotto M, Leppik R, Saudek V. 1993. Gradient-tailored water suppression for ^{1}H-^{15}N HSQC experiments optimized to retain full sensitivity. *J Magn Reson Ser A 102*:241–245.

Stryer L. 1965. The interaction of a naphthalene dye with apomyoglobin and apohemoglobin. A fluorescent probe of non-polar binding sites. *J Mol Biol 13*:482–495.

Takano T. 1977a. Structure of myoglobin refined at 2.0 Å resolution. I. Crystallographic refinement of sperm whale metmyoglobin. *J Mol Biol 110*:537–568.

Takano T. 1977b. Structure of myoglobin refined at 2.0 Å resolution. II. Structure of deoxymyoglobin from sperm whale. *J Mol Biol 110*:569–584.

Takano T. 1984. Refinement of myoglobin and cytochrome *c*. In: *Methods and applications in crystallographic computing*. Oxford, United Kingdom: Oxford University Press. pp 262–272.

Teale FWJ. 1959. Cleavage of heme-protein link by acid methylethylketone. *Biochim Biophys Acta 35*:543.

Thèriault Y, Pochapsky TC, Dalvit C, Chiu ML, Sligar SG, Wright PE. 1994. ^{1}H and ^{15}N resonance assignments and secondary structure of the carbon monoxide complex of sperm whale myoglobin. *J Biomol NMR 4*:491–504.

Torda AE, Scheek RM, van Gunsteren WF. 1990. Time-averaged nuclear Overhauser effect distance restraints applied to tendamistat. *J Mol Biol 214*:223–235.

Venable RH, Pastor RW. 1988. Frictional models for stochastic simulations of proteins. *Biopolymers 27*:1001–1004.

Wishart DS, Bigam CG, Yao J, Abildgaard F, Dyson HJ, Oldfield E, Markley JL, Sykes BD. 1995. ^{1}H, ^{13}C and ^{15}N chemical shift referencing in biomolecular NMR. *J Biomol NMR 6*:135–140.

Yang F, Phillips GNJ. 1996. Crystal structures of CO-, deoxy- and metmyoglobins at various pH values. *J Mol Biol 256*:762–774.

Zhong M, Lin L, Kallenbach NR. 1995. A method for probing the topography and interactions of proteins: Footprinting of myoglobin. *Proc Natl Acad Sci USA 92*:2111–2115.